Steel and Composite Structures, *Vol. 30, No. 4 (2019) 327-336*
DOI: https://doi.org/10.12989/scs.2019.30.4.327

Nonlinear behavior of fiber reinforced cracked composite beams

Şeref D. Akbaş*

Department of Civil Engineering, Bursa Technical University, Yıldırım Campus, Yıldırım, Bursa 16330, Turkey

(*Received January 2, 2019, Revised February 13, 2019, Accepted February 14, 2019*)

Abstract. This paper presents geometrically nonlinear behavior of cracked fiber reinforced composite beams by using finite element method with and the first shear beam theory. Total Lagrangian approach is used in the nonlinear kinematic relations. The crack model is considered as the rotational spring which separate into two parts of beams. In the nonlinear solution, the Newton-Raphson is used with incremental displacement. The effects of fibre orientation angles, the volume fraction, the crack depth and locations of the cracks on the geometrically nonlinear deflections of fiber reinforced composite are examined and discussed in numerical results. Also, the difference between geometrically linear and nonlinear solutions for the cracked fiber reinforced composite beams.

Keywords: fiber reinforced composite; geometrically nonlinear analysis; beams; crack; finite element method; total Lagrangian

1. Introduction

Fiber reinforced composite structures (FRC) are preferred to a lot of engineering projects, such as aeroplanes, defence industries, space vehicles, marine, automotive and civil engineering applications because of their higher strength-weight ratios, more lightweight and ductile properties. With the great advances in technology, the using of FRC structures is growing. FRC structures can be subjected to failure effects during the production phase or lifetime within delamination, interalaminar fracture, matrix cracking, fatigue failure, fiber breakage etc.. Cracks in a structure cause to local losing and reduction of stiffness. Due to cracks, the static and dynamic results are changed seriously. So, learning and determining of failure behavior of cracked structural members are inevitable. In a lot of papers, the linear analysis of cracked composite beams is investigated in the open literature. However, nonlinearity of composite beams with crack has not been studied broadly. In the literature, investigations of the nonlinear behavior of cracked composite beams are as follows; Nikpour and Dimarogonas (1988) investigated the energy release rate and the local compliance matrix of anisotropic materials with crack. Ghoneam (1995) examined dynamic characteristics of laminated composite beams. Shi and Hull (1992) investigated delamination fractures of composite laminates. Krawczuk and Ostachowicz (1995) studied vibrations of cracked composite beams. Toya *et al*. (1997) analyzed bending behavior of layered cracked beam. Borneman *et al*. (2009) analyzed vibration of laminated beams. Na and Reddy (2010) studied the finite element model of cracked laminated beams based on the layerwise theory. Sun and Zhou (2012) investigated the dynamics of composite beams with crack by using spectral finite element method. Karaagac *et al*. (2013) investigated buckling and vibration of laminated beams. Daneshmehr *et al*. (2013) investigated dynamics of composite beams with cracks in both bending and torsion effects. Akgöz and Civalek (2011), Ebrahimi and Hosseini (2017), Civalek (2013), Benselama *et al*. (2015), Bayat *et al*. (2015), Menasria *et al*. (2017) investigated mechanics of laminated composite structures. Akbaş (2015a, b) analyzed post-buckling of cracked Timoshenko beams. Fan and Wang (2017) examined nonlinear dynamics of laminated beams reinforced carbon nanotubes with matrix crack under thermal environment. Jena *et al*. (2016) analyzed dynamic behavior of cracked fiber reinforced composite beams. Lal *et al*. (2017) investigated fracture behavior of cracked laminated beams.

Akbaş (2018a, b, c, d, e) investigated nonlinear and post-buckling of composite beams. Akgöz and Civalek (2011), Chen and Li (2013), Farokhi *et al*. (2013), Kocatürk and Akbaş (2010), Ghayesh *et al*. (2013a, b, c, 2018), Gholipour *et al*. (2015), Farokhi and Ghayesh (2015a, b, 2018a, b), Ghayesh and Farokhi (2015), Pour *et al*. (2015), Demir *et al*. (2016), Ghayesh (2018) investigated nonlinear analysis of composite structures with different numerical methods.

As seen from literature study, geometrically nonlinear investigations of cracked composite beams have not been studied at large. The distinctive feature of this study is geometrically nonlinear bending analysis of composite laminated beams with full geometric non-linearity. In the nonlinear studies of FRC beams, the total Lagrangian approach is used not used so far. The objective of presented paper is to fill this blank for cracked FRC beams. In this study, geometrically nonlinear analysis of FRC beams is investigated within the total Lagrangian approach and first

*Corresponding author, Ph.D.,
E-mail: serefda@yahoo.com

ISSN: 1229-9367 (Print), 1598-6233 (Online)

shear beam theory by using finite element method.

The effects of fibre orientation angles, the volume fraction, the crack depth, locations of cracks on the geometrically nonlinear deflections of the FRC beams are investigated in both linear and nonlinear analysis.

2. Theory and formulation

A simply supported FRC beam with edge crack under a point load (*F*) at the midpoint is shown in Fig. 1. The depth of crack is indicated *a* and located a distance L_{cr} from the left end. The length, width and height of the beam are indicated as *L*, *b*, and *h*, respectively.

In the deriving of the nonlinear kinematic formulations, the Total Lagrangian (TL) model is used with the finite element formulations of a two-node beam element in the first shear beam theory which consist of shear deformation effects. The finite beam element with two nodes is shown in Fig. 2. The freedom degrees of the each node are horizontal displacement *u*, vertical displacement *v* and the rotation *φ*.

In the TL kinematic model, all quantities of the body are expressed as functions of initial coordinate system (*X*, *Y*). So, the final coordinates of any point (*B*) of the beam at the deformed configuration (*x*, *y*) are as follows

$$x = X + u - Ysin \tag{1}$$

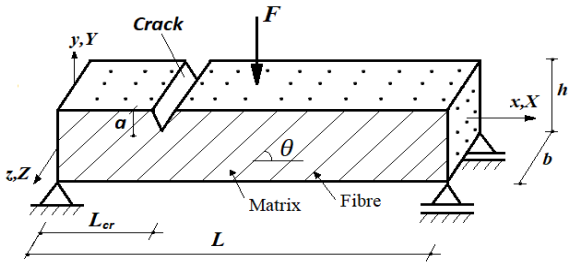

Fig. 1 A cracked simply supported FRC beam subjected to point load (*F*) at the midpoint

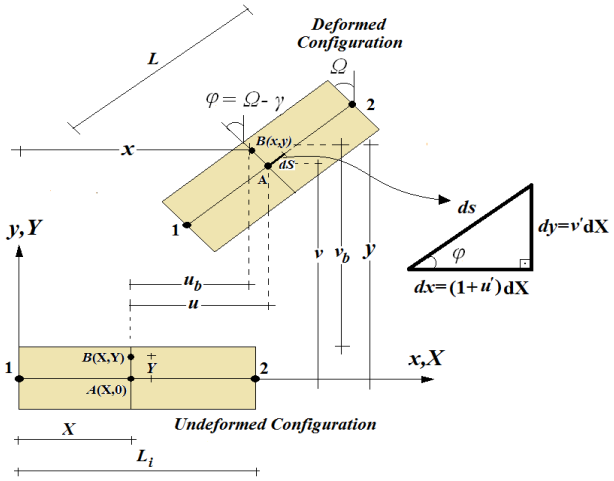

Fig. 2 The kinematics and coordinates of the beam element in the Lagrangian approach

$$y = v + Ycos\varphi \tag{2}$$

In the deformed configuration as seen from Fig. 2, the differential arc length *ds*-displacement relations are given as follows

$$ds = \sqrt{(1+u')^2 + (1+v')^2}\, dX \tag{3}$$

$$1 + u' = \frac{L\, cos\varphi}{L_i}, \quad v' = \frac{L\, sin\varphi}{L_i}, s' = \frac{L}{L_i} \tag{4}$$

The deformation gradient matrix (***F***) can be obtained as

$$[\boldsymbol{F}] = \begin{bmatrix} 1 + u' - Y\kappa\, cos\varphi & -sin\varphi \\ v' - Y\kappa\, sin\varphi & cos\varphi \end{bmatrix} \tag{5}$$

The Green-Lagrange strain tensor is as follows

$$[\boldsymbol{\epsilon}] = \tfrac{1}{2}[\boldsymbol{F^T F} - \boldsymbol{I}] \tag{6}$$

where ***I*** indicates the identity matrix. With using a consistent-linearization technique, the Green-Lagrange strain-displacement relation can be obtained as follows

$$\{\epsilon\} = \begin{Bmatrix} \epsilon_{XX} \\ 2\epsilon_{XY} \end{Bmatrix} = \begin{Bmatrix} \epsilon_{XX} \\ \gamma \end{Bmatrix} = \begin{Bmatrix} (1+u')cos\varphi + v'\, sin\varphi - Y\kappa - 1 \\ (1+u')sin\varphi + v'\, sin\varphi \end{Bmatrix} = \begin{Bmatrix} e - Y\kappa \\ \gamma \end{Bmatrix} \tag{7}$$

where ϵ_{XX}, γ, $\kappa = \varphi'$ are the axial strain, the shear strain and the curvature, respectively. In Eq. (7)

$$e = (1+u')cos\varphi + v'\, sin\varphi - 1.$$

The finite element model of the problem is shown in Fig. 3. Each node of the finite element has three freedom degrees and the displacement vector $\{\boldsymbol{u}\}^{(e)}$ for a finite element is given as follows

$$\{u\}^{(e)} = [\, u_1,\, v_1,\, \varphi_1,\, u_2,\, v_2,\, \varphi_2 \,]^T \tag{8}$$

The displacement fields ($\{\boldsymbol{u}\}^{(e)}$) of a finite beam element are given in terms of the node displacements as follows

$$u_x^{(e)} = N_1^{(u)} u_1 + N_2^{(u)} u_2 = \left[N^{(u)}\right] \begin{Bmatrix} u_1 \\ u_2 \end{Bmatrix} \tag{9}$$

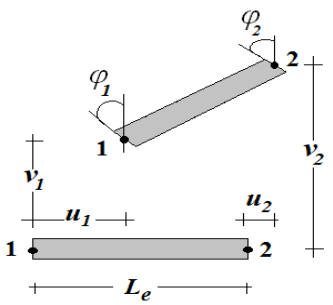

Fig. 3 Finite beam element model

$$u_y^{(e)} = N_1^{(v)} v_1 + N_2^{(v)} \varphi_1 + N_3^{(v)} v_2 + N_4^{(v)} \varphi_2 = \left[N^{(v)}\right] \begin{Bmatrix} v_1 \\ \varphi_1 \\ v_2 \\ \varphi_2 \end{Bmatrix} \quad (10)$$

$$\varphi^{(e)} = N_1^{(\varphi)} v_1 + N_2^{(\varphi)} \varphi_1 + N_3^{(\varphi)} v_2 + N_4^{(\varphi)} \varphi_2 = \left[N^{(\varphi)}\right] \begin{Bmatrix} v_1 \\ \varphi_1 \\ v_2 \\ \varphi_2 \end{Bmatrix} \quad (11)$$

where $N_{\mathrm{i}}^{(u)}$, $N_{\mathrm{i}}^{(v)}$ and $N_{\mathrm{i}}^{(\varphi)}$ are the interpolation functions for axial displacement, vertical displacement and rotation, respectively. The interpolation functions are given in appendix. The strain-displacement relation is presented with the nodal displacements in matrix form

$$\{\epsilon\} = [D]\{u\}^{(e)} \quad (12)$$

where $[D]$ is a differential operator matrix which related between the strain and the displacement vector. With using linear interpolation functions, the differential operator is given as follows

$$[D] = \frac{1}{L_i} \begin{bmatrix} -cos\varphi & -sin\varphi & \gamma N_2^{(\varphi)} L_i & cos\varphi & sin\varphi & \gamma N_4^{(\varphi)} L_i \\ sin\varphi & -cos\varphi & -N_2^{(\varphi)}(1+e)L_i & -sin\varphi & cos\varphi & -N_4^{(\varphi)}(1+e)L_i \\ 0 & 0 & -1 & 0 & 0 & 1 \end{bmatrix} \quad (13)$$

The second Piola-Kirchhoff stresses - the Green-Lagrange strain relation is given for linear elastic material as follows

$$\{\boldsymbol{S}\} = \begin{Bmatrix} S_{XX} \\ S_{XY} \end{Bmatrix} = \begin{bmatrix} \bar{Q}_{11} & \bar{Q}_{16} \\ \bar{Q}_{16} & \bar{Q}_{66} \end{bmatrix} \begin{Bmatrix} \epsilon_{XX} \\ \gamma \end{Bmatrix} = [C]\{\epsilon\}, \quad (14a)$$

$$[C] = \begin{bmatrix} \bar{Q}_{11} & \bar{Q}_{16} \\ \bar{Q}_{16} & \bar{Q}_{66} \end{bmatrix} \quad (14b)$$

where $\bar{Q}_{ij}$ are the transformed components of the reduced constitutive tensor. The transformed components of the reduced constitutive tensor for orthotropic material are as follows

$$\overline{Q}_{11} = Q_{11} l^4 + 2(Q_{12} + 2Q_{66}) l^2 n^2 + Q_{22} n^4 \quad (15a)$$

$$\overline{Q}_{12} = (Q_{11} + Q_{22} - 4Q_{66}) sin^2 cos^2 + Q_{12}(l^4 + n^4) \quad (15b)$$

$$\overline{Q}_{16} = (Q_{11} - Q_{12} - 2Q_{66}) n l^3 + (Q_{12} - Q_{22} + 2Q_{66}) n^3 l \quad (15c)$$

$$\overline{Q}_{22} = Q_{11} n^4 + 2(Q_{12} + 2Q_{66}) n^2 l^2 + Q_{22} l^4 \quad (15d)$$

$$\overline{Q}_{26} = (Q_{11} - Q_{12} - 2Q_{66}) n^3 l + (Q_{12} - Q_{22} + 2Q_{66}) n l^3 \quad (15e)$$

$$\overline{Q}_{66} = (Q_{11} + Q_{22} - 2Q_{12} - 2Q_{66}) n^2 l^2 + Q_{66}(n^4 + l^4) \quad (15f)$$

where $l = \cos\theta$ and $n = \sin\theta$, θ indicates the fiber orientation angle and the expressions of $\bar{Q}_{ij}$ are as follows

$$Q_{11} = \frac{E_1}{1 - \nu_{12}\nu_{21}}, \quad Q_{22} = \frac{E_2}{1 - \nu_{12}\nu_{21}} \quad (16a)$$

$$Q_{12} = \frac{\nu_{12} E_2}{1 - \nu_{12}\nu_{21}} = \frac{\nu_{21} E_1}{1 - \nu_{12}\nu_{21}} \quad (16b)$$

$$Q_{21} = \frac{\nu_{12} E_2}{1 - \nu_{12}\nu_{21}} = \frac{\nu_{21} E_1}{1 - \nu_{12}\nu_{21}} \quad (16c)$$

$$Q_{66} = G_{12} \quad (16d)$$

where E_1 is the Young's modulus in the *X* direction, E_2 is the Young's modulus in the *Y* direction, ν_{12} and ν_{21} are Poisson's ratios and G_{12} is the shear modulus in *XY* plane. The gross mechanical properties of the composite materials are calculated by using the following expression (Vinson and Sierakowski 2002)

$$E_1 = E_f \ V_f + E_m \left(1 - V_f\right), \quad (17a)$$

$$E_2 = E_m \left[\frac{E_f + E_m + \left(E_f - E_m\right)V_f}{E_f + E_m - \left(E_f - E_m\right)V_f}\right] \quad (17b)$$

$$\nu_{12} = \nu_f \ V_f + \nu_m \left(1 - V_f\right), \quad (17c)$$

$$G_{12} = G_m \left[\frac{G_f + G_m + \left(G_f - G_m\right)V_f}{G_f + G_m - \left(G_f - G_m\right)V_f}\right] \quad (17d)$$

where *f* indicates the fibre and *m* indicates the matrix. V_f is the volume fraction of fiber. *E*, *G* and *v* are the Young's modulus, the shear modulus and Poisson's ratio, respectively.

In Eq. (14), S_{XX} and S_{XY} the second Piola-Kirchhoff stresses axial and shear components, respectively. Substituting Eq. (12) into Eq. (14), the constitutive relation is expressed as follows

$$\{\boldsymbol{S}\} = [C][D]\{u\}^{(e)} \quad (18)$$

The virtual work equation of the beam element based on the TL approach with neglecting the body forces is given as follows

$$\int_V (s_{XX}\delta\varepsilon_{XX} + s_{XY}\delta\gamma) dV - \int_0 (r_X \delta u + r_Y \delta v) dS = 0 \quad (19a)$$

$$\int_V \{\boldsymbol{S}\}\{\delta\epsilon\} dV - \int_S \left\{\delta u^{(e)}\right\}^T [N]^T \begin{Bmatrix} r_X \\ r_Y \end{Bmatrix} dS = 0 \quad (19b)$$

where r_X and r_Y are the boundary forces in the *X* and *Y* directions respectively. *V* indicates the volume of the body. Substituting Eqs. (18) and (12) into Eq. (19b) and applying

the variational process, the virtual work equation is expressed as follows

$$\int_V \left([C][D]\{u\}^{(e)}\right)\left(\frac{\partial[D]}{\partial u}\{\delta u\}^{(e)} + [D]\{\delta u\}^{(e)}\right) dV \int_0^{L_e} \{\delta u^{(e)}\}^T [N]^T \begin{Bmatrix} r_X \\ r_Y \end{Bmatrix} dX = 0 \tag{20a}$$

$$\{\delta u\}^{(e)}\left(\int_V \left(\frac{\partial[D]^T}{\partial u}[C][D] + [D]^T[C][D]\right)\{u\}^{(e)} dV \int_0^{L_e} [N]^T \begin{Bmatrix} r_X \\ r_Y \end{Bmatrix} dX\right) dX = 0 \tag{20b}$$

After integration process and the regulation of the Eq. (20b), the equation of motion is expressed as follows

$$\{u\}^{(e)}\left(\int_0^{L_e} \left(\frac{\partial[D]^T}{\partial u}[C][D]A + [D]^T[C][D]A\right) dX - \int_0^{L_e} [N]^T \begin{Bmatrix} r_X \\ r_Y \end{Bmatrix} dX\right) = 0 \tag{21}$$

In Eq. (21), $\{u\}^{(e)}$ is the displacement vector. The element tangent stiffness matrix is presented as follows

$$\boldsymbol{K}_T = \boldsymbol{K}_M + \boldsymbol{K}_G \tag{22}$$

where $\boldsymbol{K}_G$ and $\boldsymbol{K}_M$ are the geometric and material stiffness matrixes, respectively, as follows

$$\boldsymbol{K}_M = \int_0^{L_e} [D]^T[C][D]A\, dX \tag{23a}$$

$$\boldsymbol{K}_G = \int_0^{L_e} \frac{\partial[D]^T}{\partial u}[C][D]A\, dX \tag{23b}$$

The load vector $\boldsymbol{F}$ is given as follows

$$\boldsymbol{F} = \int_0^{L_e} [N]^T \begin{Bmatrix} r_X \\ r_Y \end{Bmatrix} dX \tag{24}$$

In the nonlinear finite element solution, Newton-Raphson iteration procedure is considered. In solution procedure, the load is divided by an appropriate number with the small-step incremental. For n+1 st load increment and i th iteration, increment displacement vector is given as follows

$$d\boldsymbol{u}_n^i = \left(\boldsymbol{K}_T^i\right)^{-1} \boldsymbol{F}_{n+1}^i \tag{25}$$

where $\boldsymbol{K}_T^i$, $d\boldsymbol{u}_n^i$ and $\boldsymbol{F}_{n+1}^i$ are the tangent stiffness matrix, the increment displacement vector and the load vector respectively for i th iteration and n+1 st load increment. The iteration tolerance form is selected in the Euclidean norm as follows

$$\sqrt{\frac{[(d\boldsymbol{u}_n^{i+1} - d\boldsymbol{u}_n^i)^T(d\boldsymbol{u}_n^{i+1} - d\boldsymbol{u}_n^i)]^2}{[(d\boldsymbol{u}_n^{i+1})^T(d\boldsymbol{u}_n^{i+1})]^2}} \le \xi_{tol} \tag{26}$$

The updated displacement vector after the end of the i th iteration and n+1 st load increment is given as follows

$$\boldsymbol{u}_{n+1}^{i+1} = \boldsymbol{u}_{n+1}^i + d\boldsymbol{u}_{n+1}^i = \boldsymbol{u}_n + \Delta\boldsymbol{u}_n^i \tag{27}$$

where

$$\Delta\boldsymbol{u}_n^i = \sum_{k=1}^{i} d\boldsymbol{u}_n^k \tag{28}$$

The crack model is considered in the rotational spring which separate into two parts of beams shown in Fig. 4.

Due to the crack, the flexibility coefficient (f_{ij}) depend on the stress intensity and crack modes is given as follows (Tada *et al*. 1985)

$$f_{ij} = \frac{\partial^2 U_a}{\partial P_i \partial P_j} \tag{29}$$

where U indicates the additional strain energy due to the crack and P indicates the load. The additional strain energy U_a is presented with the stress intensity factor according to fracture mode *1* as follows (Nikpur and Dimarogonas 1988)

$$U_a = \int_A D_1 \sum_{i=1}^{4} K_{Ii}\, dA \tag{30}$$

where K_I is the stress intensity factors for fracture mode 1, i indicates the effects of the loads on the stress intensity factor. D_1 is the parameters that depends the material constants as follows (Nikpur and Dimarogonas 1988)

$$D_1 = -0.5\, \bar{C}_{22}\, I_m\left(\frac{S_1 + S_2}{S_1 S_2}\right) \tag{31}$$

where I_m indicates the imaginary, S_1 and S_2 are the roots results of following equation (Vinson and Sierakowski 2002)

$$C_{11}S^4 - 2\bar{C}_{16}S^3 + (2\,\bar{C}_{12} + \bar{C}_{66})S^2 - 2\,\bar{C}_{26}S + \bar{C}_{22} = 0 \tag{32}$$

where $\bar{C}_{ij}$ constants are given as follows (Vinson and Sierakowski 2002)

$$\bar{C}_{11} = c_{11}m^4 + (2c_{12} + c_{66})l^2n^2 + b_{22}n^4 \tag{33a}$$

$$\bar{C}_{22} = c_{11}n^4 + (2c_{12} + c_{66})l^2n^2 + c_{22}l^4 \tag{33b}$$

$$\bar{C}_{12} = (c_{11} + c_{22} - c_{66})l^2n^2 + c_{12}(l^4 + n^4) \tag{33c}$$

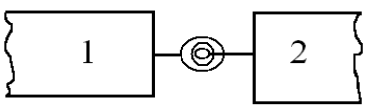

Fig. 4 Cracked FRC beam with rotational spring

$$\bar{C}_{16} = (-2c_{11} + 2c_{12} + b_{66})l^3 n + (2c_{22} - 2c_{12} - c_{66})ln^3 \quad (33d)$$

$$\bar{C}_{26} = (-2c_{11} + 2c_{12} + c_{66})ln^3 + (2c_{22} - 2c_{12} - c_{66})l^3 n \quad (33e)$$

$$\bar{C}_{66} = 2(2c_{11} - 4c_{12} + 2c_{22} - c_{66})l^2 n^2 + c_{66}(l^4 + n^4) \quad (33f)$$

where $l = \cos\theta$ and $n = \sin\theta$, θ indicates fiber orientation angle. b_{ij} indicates material constants as follows (Vinson and Sierakowski 2002)

$$c_{11} = \frac{1}{E_{11}}\left(1 - \frac{E_{22}}{E_{11}}\nu_{12}^2\right), \quad c_{22} = \frac{1}{E_{22}}\left(1 - \frac{E_{22}}{E_{11}}\nu_{23}^2\right)$$
$$c_{12} = -\frac{\nu_{12}}{E_{11}}(1 + \nu_{23}), \quad c_{44} = \frac{1}{G_{23}}, \quad (34)$$
$$c_{55} = \frac{1}{G_{12}}, \quad c_{66} = c_{55}$$

The stress intensity factors K_I for fracture mode 1 is expressed as follows

$$K_{IM} = \frac{6M}{bH^2}\sqrt{\pi a}\, Y_1 \quad (35)$$

Where a indicates the crack depth, M is the bending moment and Y_1 is the correction factor for anisotropic material (Tada *et al*. 1985)

$$Y_1 = \sqrt{\frac{tan\lambda}{\lambda}}[0{,}923 + 0{,}199(1 - sin\lambda)^4]\frac{C_1\{\xi\}}{cos\lambda} \quad (36)$$

where $\lambda = \pi a/2H$ and $C_1\{\xi\}$ is given as follows

$$C_1\{\xi\} = 1 + 0.1(\xi - 1) - 0.16(\xi - 1)^2 + 0.002(\xi - 1)^3 \quad (37)$$

where $\xi = \sqrt{E_{11}E_{22}}\Big/2G_{12} - \nu_{12}$.

Substituting the Eqs. (35) and (31) into Eq. (30), and after using the Eq. (29), the flexibility coefficient f at the crack section can be expressed as follows

$$f = \frac{72\,\pi\, D_1}{bH^4}\int_0^{a_r} a\, Y_I^2\, da \quad (38)$$

where a_r is the crack depth ratios which defined as follows

$$a_r = a/h \quad (39)$$

At the crack section, with using the inverse of the flexibility coefficient *f*, the stiffness k_T and the stiffness matrix $[K]_{cr}$ can be expressed as follows

$$k_T = \frac{1}{f} \quad (40)$$

$$[K]_{cr} = \begin{bmatrix} k_T & -k_T \\ -k_T & k_T \end{bmatrix} \quad (41)$$

According to spring model for the crack, the boundary conditions at crack section are given as follows

$$u_L = u_R, \quad v_L = v_R, \quad N_L = N_R,$$
$$T_L = T_R, \quad M_L = M_R, \quad \varphi_L - \varphi_R = \frac{M}{k_T} \quad (42)$$

where u is the horizontal displacement, v is the vertical displacement, N is the normal force, T is the shear force, M is moment, φ is the rotation, R indicates the right side of the crack and L indicates the left side of the crack. The displacement vector in the crack section is given as follows

$$\{u\}_{cr} = \{\varphi_L \quad \varphi_R\} \quad (43)$$

With adding the stiffness matrix at the crack section, the total stiffness matrix for cracked beam is presented as follows

$$\boldsymbol{K}_T = \boldsymbol{K}_M + \boldsymbol{K}_G + [\boldsymbol{K}]_{\boldsymbol{cr}} \quad (44)$$

3. Numerical results

In the numerical results, geometrically nonlinear static deflections of cracked FRC simply supported beams are obtained in figures for different fibre orientation angles, volume fraction, the crack depth and the crack locations. Difference between nonlinear and linear analysis is investigated. The FRC beam considered is made of graphite fibre-reinforced polyamide composite in numerical examples. Material parameters of graphite fibre-reinforced polyamide composite are as follows (Krawczuk *et al* 1997, Kısa 2004) with matrix and fibre properties values; E_m = 2.756 GPa, E_f = 275.6 GPa, G_m = 1.036 GPa, G_f = 114.8 GPa, ν_m = 0.33, ν_f = 0.2. The geometry parameters of FRC beam are selected as; b = 0.2 m, h = 0.2 m and L = 4 m. In integration process, five-point Gauss rule is used. The number of finite elements is taken as 100 in the numerical calculations.

In Fig. 5, effect of crack depth ratios (a_r) on maximum vertical displacements (at the midpoint) of FRC beam is presented with load rising for different a_r for the crack location L_{cr} = 0.4L, the fiber orientation angle $\theta = 10^\circ$, the volume fraction of fiber V_f = 0.1 in both linear and nonlinear results. Also, the effect of a_r on the deflection shapes is presented in figure 6 for $\theta = 30^\circ$, V_f = 0.2, L_{cr} = 0.3L, F = 500 kN in both nonlinear and linear results.

It is obvious from this Fig. 5 that increasing the a_r yields increasing of the displacements, naturally. In higher load values, the effects of the crack more increase. The difference between nonlinear and linear solution increases with increasing the load. The results of linear solution are bigger than in the nonlinear's for all a_r values. The effect of a_r can be clearly seen in Fig. 6. Difference between the geometrically nonlinear and linear deflections of FRC beam is quite large in deformed configurations.

In Fig. 7, the relationship between crack depth ratios

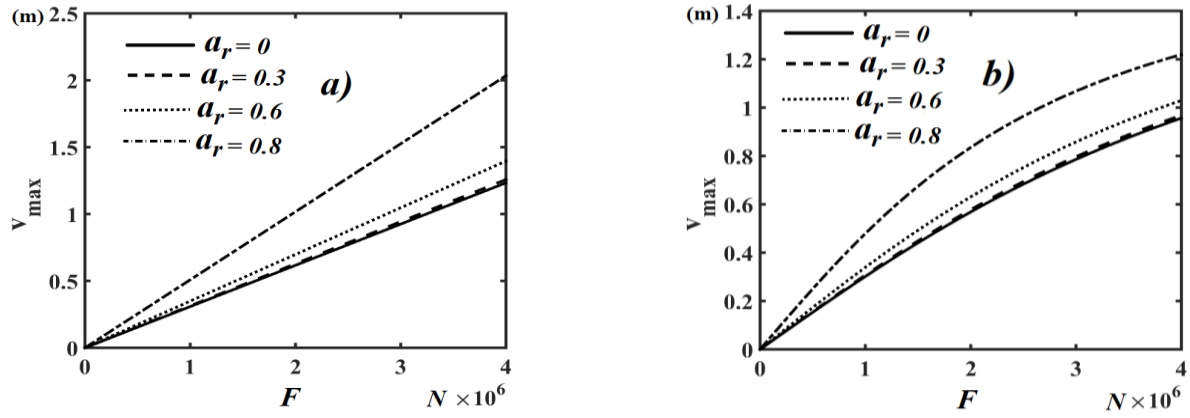

(a) Linear solution (b) Nonlinear solution

Fig. 5 Load- maximum deflections curves for different a_r values

0 . 5 L , F =

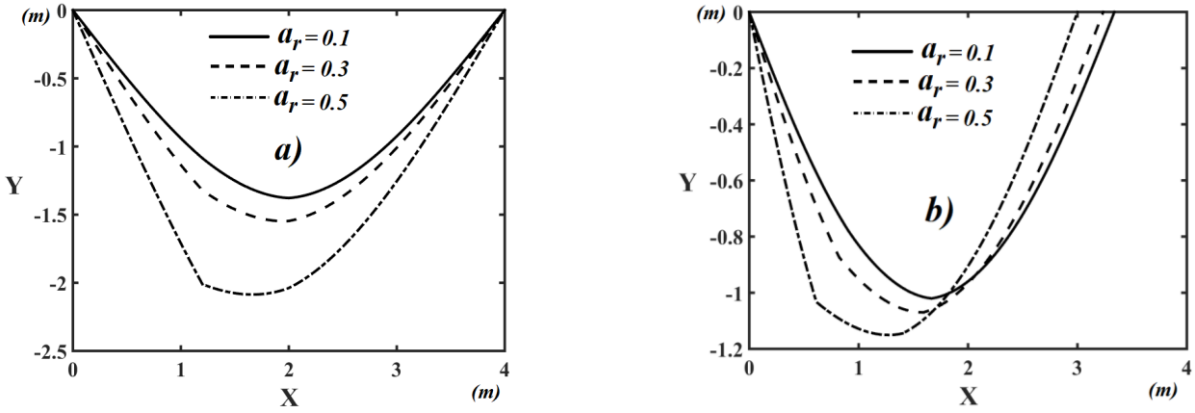

(a) Linear solution (b) Nonlinear solution

Fig. 6 Effect of a_r on displacement configuration of FRC beam

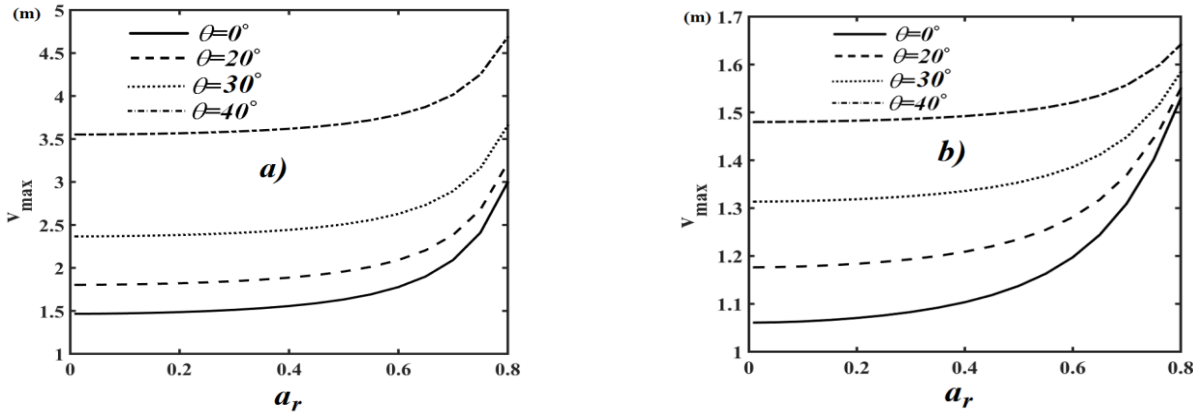

(a) Linear solution (b) Nonlinear solution

Fig. 7 The relationship between the crack depth ratios (a_r) and maximum deflections (v_{max}) for different values θ

(a_r) and the maximum vertical displacements (at the midpoint) is plotted for different fiber orientation angles (θ)values for V_f = 0.1, L_{cr} = 0.5L, F = 500 kN in both nonlinear and linear results. In Fig. 8, the effect of θ on the deflection shapes is presented for a_r = 0.5, V_f = 0.1, L_{cr} = 500 kN in both nonlinear and linear results.

Fig. 7 displays that increasing the fiber orientation angles, the deflections of the composite beam increase significantly in both linear and nonlinear solutions. According to the Eq. (15), the bending rigidity decreases with increasing the fiber orientation angles. So, the strength of beam decreases and deflections increase naturally with

increasing the fiber orientation angles. This situation can be clearly seen in Fig. 8. The difference among fiber orientation angles decrease considerably increasing in the crack depth ratios (a_r). Also, the displacements for different θ values fast converge in the nonlinear solution in contrast with linear solution. The fiber orientation angle is very effective in the nonlinear solution in contrast with linear solution. It shows that the difference between the geometrically nonlinear and linear deflections of FRC beam change considerably with increasing the a_r and θ.

In Fig. 9, the relationship between crack depth ratios (a_r) and the maximum vertical displacements is plotted for different volume fraction of fiber V_f values for $\theta = 20^\circ$, L_{cr} = 0.5L, F = 500 kN in both nonlinear and linear results.

Fig. 9 displays that increasing volume fraction of fiber yields to decrease deflections in the case that the crack depth ratio is less than about 0.3. However, the deflections increase with increasing the V_f for a_r > 0.3. Normally, the deflections increase with increasing the volume fraction of fiber V_f because of high strength properties of fiber. However, this situation is changed up to a value of the crack depth ratio. It shows that crack depth has important role on effects of fibers on the mechanical behavior of FRC beams. Another result of the Fig. 9 that the results of V_f converge in the nonlinear solution with increasing the a_r. However, results of V_f diverge in the linear solution with increasing the a_r. It is concluded from Fig. 9, the mechanical behavior of FRC beams considerably differs between linear and nonlinear analysis.

Fig. 10 display the displacement configuration of the FRC beam with different crack location (L_{cr}) for $\theta = 30^\circ$, $a_r = 0.5$, V_f = 0.2, F = 500 kN in both linear and nonlinear results. The crack location is based from the left end. Fig. 10 shows that crack location ratio increases, namely, the crack comes close to midpoint of FRC beam, the FRC beam more deflects. There is a big difference between deflected shapes of the FRC beam for linear and nonlinear analysis.

It is seen from the displacement configurations (Figs. 6, 8 and 10), increasing in the volume fraction of fiber, crack depth and crack locations is more effective in the vertical displacements of the linear solution because the axial displacements and axial rigidity do not occur for this problem in the linear analysis. The arm of the external

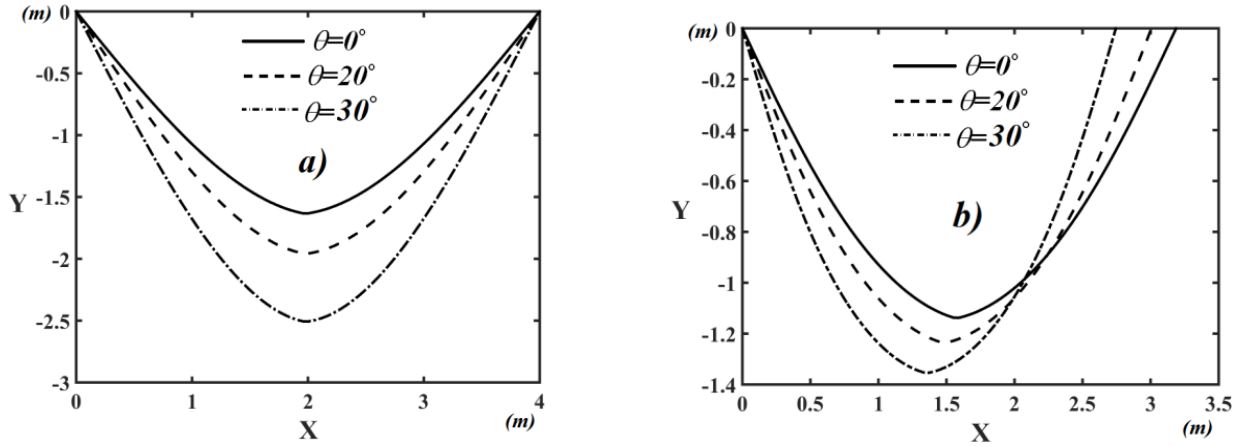

(a) Linear solution (b) Nonlinear solution

Fig. 8 Effect of θ on displacement configuration of FRC beam

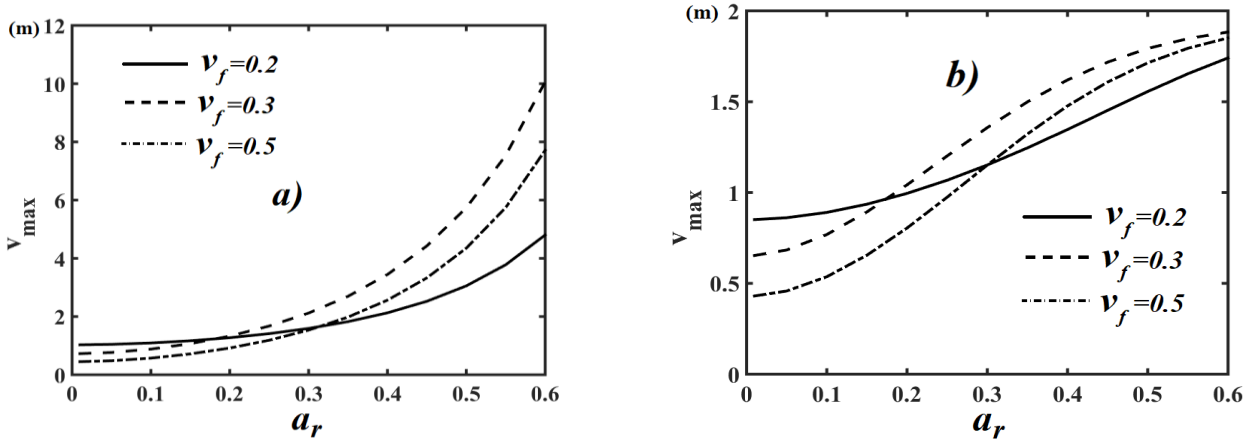

(a) Linear solution (b) Nonlinear solution

Fig. 9 The relationship between the crack depth ratios (a_r) and maximum deflections (v_{max}) for different V_f values

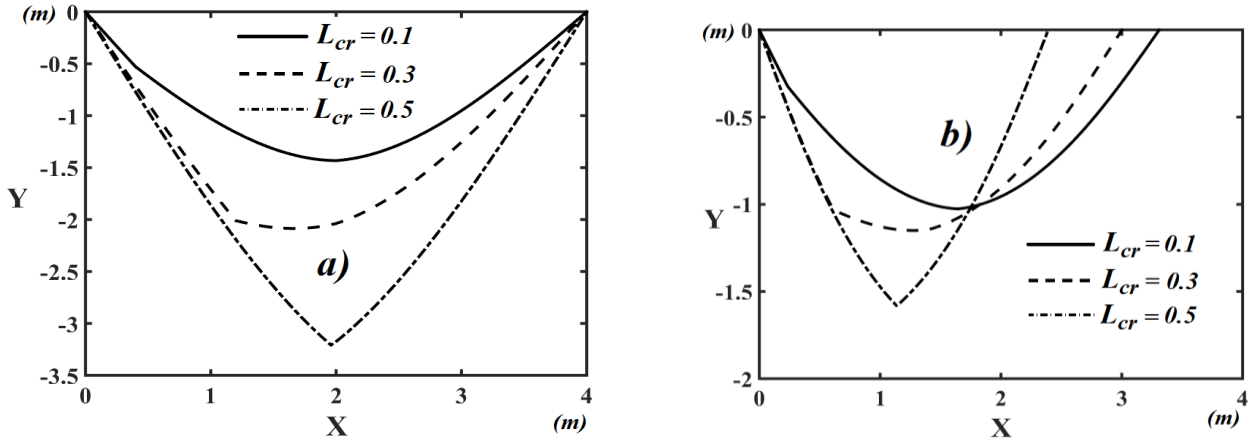

(a) Linear solution (b) Nonlinear solution

Fig. 10 The effect of crack location (L_{cr}) on displacement configuration of FRC beam

forces do not change with the load, crack and material parameters. However, this situation is completely different in the nonlinear analysis. In the nonlinear analysis, the arm of the external forces change with the load, crack and material parameters. After certain load, crack and material parameters level in which the configuration of the beam is close to the vertical direction and axial rigidity gains more importance than its flexural rigidity. It shows that there is completely difference between the linear and nonlinear analysis after load, crack and material parameters level. So, the nonlinear analysis must be used in the higher values of the load, crack and material parameters in order to obtain more realistic results for FRC beams.

4. Conclusions

Geometrically nonlinear deflections of FRC simply supported cracked beams are investigated based finite element method within the first shear beam theory. In the nonlinear kinematic model, the total Lagrangian approach is used. The rotational spring crack model is used in the crack model. In solution of the nonlinear problem, the Newton-Raphson method is used. Effects of fibre orientation angles, volume fraction, crack depth locations on the geometrically nonlinear deflections of the FRC beams are investigated. Also, linear analysis deflections are presented and compared with nonlinear deflections. It is concluded from the numerical results, the main results are as follows:

- The crack depth is very effective in non-linear behaviour of cracked FRC beam.
- The deflections of linear solution are bigger than in the nonlinear's.
- Difference between the geometrically nonlinear and linear deflections of FRC beam is quite large in higher load values, material and crack parameters.
- The fiber orientation angle is very effective in the nonlinear solution in contrast with linear solution.
- The crack depth has important role on the effects of fibers on mechanical behavior of FRC beams.

It is necessary to use the nonlinear analysis for higher values of load, crack and material parameters in the FRC beams.

References

Akbaş, Ş.D. (2015a), "On post-buckling behavior of edge cracked functionally graded beams under axial loads", *Int. J. Struct. Stabil. Dyn.*, **15**(4), 1450065.

Akbaş, Ş.D. (2015b), "Large deflection analysis of edge cracked simple supported beams", *Struct. Eng. Mech., Int. J.*, **54**(3), 433-451.

Akbaş, Ş.D. (2018a), "Nonlinear Thermal Displacements of Laminated Composite Beams", *Coupl. Syst. Mech., Int. J.*, *7*(6), 691-705.

Akbaş, Ş.D. (2018b), "Thermal Post-Buckling Analysis of a Laminated Composite Beam", *Struct. Eng. Mech., Int. J.*, **67**(4), 337-346.

Akbaş, Ş.D. (2018c), "Large Deflection Analysis of a Fiber Reinforced Composite Beam", *Steel Compos. Struct., Int. J.*, **27**(5), 567-576.

Akbaş, Ş.D. (2018d), "Geometrically Nonlinear Analysis of a Laminated Composite Beam", *Struct. Eng. Mech., Int. J.*, **66**(1), 27-36.

Akbaş, Ş.D. (2018e), "Post-Buckling Responses of a Laminated Composite Beam , *Steel Compos. Struct., Int. J.*, **26**(6), 733-743.

Akgöz, B. and Civalek, Ö. (2011), "Nonlinear vibration analysis of laminated plates resting on nonlinear two-parameters elastic foundations", *Steel Compos. Struct., Int. J.*, **11**(5), 403-421.

Bayat, R., Jafari, A.A. and Rahmani, O. (2015), "Analytical solution for free vibration of laminated curved beam with magnetostrictive layers", *Int. J. Appl. Mech.*, **7**(3), 1550050.

Benselama, K., El Meiche, N., Bedia, E.A.A. and Tounsi, A. (2015), "Buckling analysis in hybrid cross-ply composite laminates on elastic foundation using the two variable refined plate theory", *Struct. Eng. Mech., Int. J.*, **55**(1), 47-64.

Borneman, S.R., Hashemi, S.M. and Alighanbari, H. (2009), "Vibration Analysis of Cracked Stepped Laminated Composite Beams", *Int. J. Vehicle Struct. Syst.*, **1**(1), p.16.

Chen, W.J. and Li, X.P. (2013), "Size-dependent free vibration analysis of composite laminated Timoshenko beam based on new modified couple stress theory", *Arch. Appl. Mech.*, **83**, 431-444.

Civalek, Ö. (2013), "Nonlinear dynamic response of laminated plates resting on nonlinear elastic foundations by the discrete singular convolution-differential quadrature coupled

approaches", *Compos. Part B*: *Eng*., **50**, 171-179.
Daneshmehr, A.R., Nateghi, A. and Inman, D.J. (2013), "Free vibration analysis of cracked composite beams subjected to coupled bending–torsion loads based on a first order shear deformation theory", *Appl. Math. Model*., **37**(24), 10074-10091.
Demir, C., Mercan K. and Civalek, O. (2016), "Determination of critical buckling loads of isotropic, FGM and laminated truncated conical panel", *Compos. Part B*, **94**, 1-10.
Ebrahimi, F. and Hosseini, S.H.S. (2017), "Surface effects on nonlinear dynamics of NEMS consisting of double-layered viscoelastic nanoplates", *Eur. Phys. J. Plus*, **132**(4), 172.
Fan, Y. and Wang, H. (2017), "The effects of matrix cracks on the nonlinear vibration characteristics of shear deformable laminated beams containing carbon nanotube reinforced composite layers", *Int. J. Mech. Sci*., **124**, 216-228.
Farokhi, H., Ghayesh, M.H. and Amabili, M. (2013), Nonlinear dynamics of a geometrically imperfect microbeam based on the modified couple stress theory", *Int. J. Eng. Sci*., **68**, 11-23.
Farokhi, H. and Ghayesh, M.H. (2015a), "Thermo-mechanical dynamics of perfect and imperfect Timoshenko micro-beams", *Int. J. Eng. Sci*., **91**, 12-33.
Farokhi, H. and Ghayesh, M.H. (2015b), "Nonlinear dynamical behaviour of geometrically imperfect microplates based on modified couple stress theory", *Int. J. Mech. Sci*., **90**, 133-144.
Farokhi, H. and Ghayesh, M.H. (2018a), "Supercritical nonlinear parametric dynamics of Timoshenko microbeams", *Commun. Nonlinear Sci. Numer. Simul*., **59**, 592-605.
Farokhi, H. and Ghayesh, M.H. (2018b), "Nonlinear mechanics of electrically actuated microplates", *Int. J. Eng. Sci*., **123**, 197-213.
Ghayesh, M.H. (2018), "Nonlinear vibration analysis of axially functionally graded shear-deformable tapered beams", *Appl. Math. Model*., **59**, 583-596.
Ghayesh, M.H. and Farokhi, H. (2015), "Nonlinear dynamics of microplates", *Int. J. Eng. Sci*., **86**, 60-73.
Ghayesh, M.H., Farokhi, H. and Amabili, M. (2013a), "Nonlinear behaviour of electrically actuated MEMS resonators", *Int. J. Eng. Sci*., **71**, 137-155.
Ghayesh, M.H., Farokhi, H. and Amabili, M. (2013b), "Nonlinear dynamics of a microscale beam based on the modified couple stress theory", *Compos. Part B*: *Eng*., **50**, 318-324.
Ghayesh, M.H., Amabili, M. and Farokhi, H. (2013c), "Nonlinear forced vibrations of a microbeam based on the strain gradient elasticity theory", *Int. J. Eng. Sci*., **63**, 52-60.
Ghayesh, M.H., Farokhi, H., Gholipour, A. and Tavallaeinejad, M. (2018), "Nonlinear oscillations of functionally graded microplates", *Int. J. Eng. Sci*., **122**, 56-72.
Gholipour, A., Farokhi, H. and Ghayesh, M.H. (2015), "In-plane and out-of-plane nonlinear size-dependent dynamics of microplates", *Nonlinear Dyn*., **79**(3), 1771-1785.
Ghoneam, S.M. (1995), "Dynamic analysis of open cracked laminated composite beams", *Compos. Struct*., **32**(1-4), 3-11.
Jena, P.C., Parhi, D.R. and Pohit, G. (2016), "Dynamic Study of Composite Cracked Beam by Changing the Angle of Bidirectional Fibres", *Iran. J. Sci. Technol. Transactions A*: *Sci*., **40**(1), 27-37.
Karaagac, C., Ozturk, H. and Sabuncu, M. (2013), "Effects of an edge crack on the free vibration and lateral buckling of a cantilever laminated composite slender beam", *J. Vib. Control*, **19**(16), 2506-2522.
Kısa, M. (2004), "Free vibration analysis of a cantilever composite beam with multiple cracks", *Compos. Sci. Technol*., **64**(9), 1391-1402.
Kocatürk, T. and Akbaş, Ş.D. (2010), "Geometrically non-linear static analysis of a simply supported beam made of hyperelastic material", *Struct. Eng. Mech., Int. J*., **35**(6), 677-697.
Krawczuk, M. and Ostachowicz, W.M. (1995), "Modelling and vibration analysis of a cantilever composite beam with a transverse open crack", *J. Sound Vib*., **183**(1), 69-89.
Krawczuk, M., Ostachowicz, W. and Zak, A. (1997), "Modal analysis of cracked, unidirectional composite beam", *Compos. Part B*: *Eng*., **28**(5-6), 641-650.
Lal, A., Mulani, S.B. and Kapania, R.K. (2017), "Stochastic Fracture Response and Crack Growth Analysis of Laminated Composite Edge Crack Beams Using Extended Finite Element Method", *Int. J. Appl. Mech*., **9**(4), 1750061.
Menasria, A., Bouhadra, A., Tounsi, A., Bousahla, A.A. and Mahmoud, S.R. (2017), "A new and simple HSDT for thermal stability analysis of FG sandwich plates", *Steel Compos. Struct*., *Int. J*., **25**(2), 157-175.
Na, W.J. and Reddy, J.N. (2010), "Multiscale Analysis of Transverse Cracking in Cross-Ply Laminated Beams using The Layer Wise Theory", *J. Solid Mech*., **2**(1), 1-18.
Nikpur, K. and Dimarogonas, A. (1988), "Local compliance of composite cracked bodies", *Compos. Sci. Technol*., **32**(3), 209-223.
Pour, H.R., Vossough, H., Heydari, M.M., Beygipoor, G. and Azimzadeh, A. (2015), "Nonlinear vibration analysis of a nonlocal sinusoidal shear deformation carbon nanotube using differential quadrature method", *Struct. Eng. Mech., Int. J*., **54**(6), 1061-1073.
Shi, Y.B. and Hull, D. (1992), "Fracture of delaminated unidirectional composite beams", *J. Compos. Mater*., **26**(15), 2172-2195.
Sun, H. and Zhou, L. (2012), "Analysis of damage characteristics for cracked composite structures using spectral element method", *J. Vibroeng*., **14**(1), 430-439.
Tada, H., Paris, P.C. and Irwin, G.R. (1985), *The Stress Analysis of Cracks Handbook*, Paris Production Incorporated and Del Research Corporation.
Toya, M., Aritomi, M. and Chosa, A. (1997), "Energy release rates for an interface crack embedded in a laminated beam subjected to three-point bending", *J. Appl. Mech*., **64**(2), 375-382.
Vinson, J.R. and Sierakowski, R.L. (2002), "Behaviour of structures composed of composite materials", Kluwer Academic Publishers, ISBN 978-140-2009-04-4, Netherlands.

CC

Appendix

The shape functions for axial degrees of freedom are as follows

$$\varphi^{(U)}(\mathrm{X}) = \left[\varphi_1^{(U)}(\mathrm{X})\ \ \varphi_2^{(U)}(\mathrm{X})\right]^T \tag{A1}$$

where

$$\varphi_1^{(U)}(\mathrm{X}) = \left(-\frac{X}{L_\mathrm{e}} + 1\right), \quad \varphi_2^{(U)}(\mathrm{X}) = \left(\frac{X}{L_\mathrm{e}}\right), \tag{A2}$$

The shape functions for transverse degrees of freedom are as follows

$$\varphi^{(V)}(\mathrm{X}) = \left[\varphi_1^{(V)}(\mathrm{X})\ \ \varphi_2^{(V)}(\mathrm{X})\ \ \varphi_3^{(V)}(\mathrm{X})\ \ \varphi_4^{(V)}(\mathrm{X})\right]^T, \tag{A3}$$

where

$$\varphi_1^{(V)}(\mathrm{X}) = \left(1 - \frac{12X}{L_\mathrm{e}\left(12 + \frac{GA}{EI}L_\mathrm{e}^2\right)} - \frac{3\left(\frac{GA}{EI}\right)X^2}{\left(12 + \frac{GA}{EI}L_\mathrm{e}^2\right)} + \frac{2(GA/EI)X^3}{L_\mathrm{e}\left(12 + \frac{GA}{EI}L_\mathrm{e}^2\right)}\right), \tag{A4}$$

$$\varphi_2^{(V)}(\mathrm{X}) = \left(\frac{\left(6 + \frac{GA}{EI}L_\mathrm{e}^2\right)X}{\left(12 + \frac{\mu A}{EI}L_\mathrm{e}^2\right)} - \frac{\left(6 + 2\frac{GA}{EI}L_\mathrm{e}^2\right)X^2}{L_\mathrm{e}\left(12 + \frac{GA}{EI}L_\mathrm{e}^2\right)} + \frac{\frac{GA}{EI}}{6}\left(1 - \frac{\left(6L_\mathrm{e} + \frac{GA}{EI}L_\mathrm{e}^3\right)}{L_\mathrm{e}\left(12 + \frac{GA}{EI}L_\mathrm{e}^2\right)}\right)X^3\right), \tag{A5}$$

$$\varphi_3^{(V)}(\mathrm{X}) = \left(\frac{12X}{L_\mathrm{e}\left(12 + \frac{GA}{EI}L_\mathrm{e}^2\right)} + \frac{3\left(\frac{GA}{EI}\right)X^2}{\left(12 + \frac{GA}{EI}L_\mathrm{e}^2\right)} - \frac{2\left(\frac{GA}{EI}\right)X^3}{L_\mathrm{e}\left(12 + \frac{GA}{EI}L_\mathrm{e}^2\right)}\right), \tag{A6}$$

$$\varphi_4^{(V)}(\mathrm{X}) = \left(-\frac{6X}{\left(12 + \frac{GA}{EI}L_\mathrm{e}^2\right)} - \frac{\left(\frac{GA}{EI}L_\mathrm{e}^2 - 6\right)X^2}{\left(12 + \frac{GA}{EI}L_\mathrm{e}^2\right)} + \frac{\left(\frac{GA}{EI}\right)X^3}{\left(12 + \frac{GA}{EI}L_\mathrm{e}^2\right)}\right), \tag{A7}$$

The shape functions for rotation degrees of freedom are as follows

$$\varphi^{(\emptyset)}(\mathrm{X}) = \left[\varphi_1^{(\emptyset)}(\mathrm{X})\ \ \varphi_2^{(\emptyset)}(\mathrm{X})\ \ \varphi_3^{(\emptyset)}(\mathrm{X})\ \ \varphi_4^{(\emptyset)}(\mathrm{X})\right]^T, \tag{A8}$$

where

$$\varphi_1^{(\emptyset)}(\mathrm{X}) = \left(-\frac{6\left(\frac{GA}{EI}\right)X}{\left(12 + \frac{GA}{EI}L_\mathrm{e}^2\right)} + \frac{6\left(\frac{GA}{EI}\right)X^2}{L_\mathrm{e}\left(12 + \frac{GA}{EI}L_\mathrm{e}^2\right)}\right), \tag{A9}$$

$$\varphi_2^{(\emptyset)}(\mathrm{X}) = \left(1 - \frac{2\left(2\frac{GA}{EI}L_\mathrm{e}^2 + 6\right)X}{L_\mathrm{e}\left(12 + \frac{GA}{EI}L_\mathrm{e}^2\right)} + \frac{GA/EI}{2}\left(1 - \frac{\left(6L_\mathrm{e} + \frac{GA}{EI}L_\mathrm{e}^3\right)}{L_\mathrm{e}\left(12 + \frac{GA}{EI}L_\mathrm{e}^2\right)}\right)X^2\right) \tag{A10}$$

$$\varphi_3^{(\emptyset)}(\mathrm{X}) = \left(\frac{6\left(\frac{GA}{EI}\right)X}{\left(12 + \frac{GA}{EI}L_\mathrm{e}^2\right)} - \frac{6\left(\frac{GA}{EI}\right)X^2}{L_\mathrm{e}\left(12 + \frac{GA}{EI}L_\mathrm{e}^2\right)}\right), \tag{A11}$$

$$\varphi_4^{(\emptyset)}(\mathrm{X}) = \left(-\frac{2\left(\frac{GA}{EI}L_\mathrm{e}^2 - 6\right)X}{L_\mathrm{e}\left(12 + \frac{GA}{EI}L_\mathrm{e}^2\right)} + \frac{3\left(\frac{GA}{EI}\right)X^2}{\left(12 + \frac{GA}{EI}L_\mathrm{e}^2\right)}\right), \tag{A12}$$